

---

# AFFORDANCE-BASED ROBOT MANIPULATION WITH FLOW MATCHING

---

Fan Zhang, Michael Gienger  
 Honda Research Institute EU  
 firstname.lastname@honda-ri.de

December 5, 2024

## ABSTRACT

We present a framework for assistive robot manipulation, which focuses on two fundamental challenges: first, efficiently adapting large-scale models to downstream scene affordance understanding tasks, especially in daily living scenarios where gathering multi-task data involving humans requires strenuous effort; second, effectively learning robot trajectories by grounding the visual affordance model. We tackle the first challenge by employing a parameter-efficient prompt tuning method that prepends learnable text prompts to the frozen vision model to predict manipulation affordances in multi-task scenarios. Then we propose to learn robot trajectories guided by affordances in a supervised Flow Matching method. Flow matching represents a robot visuomotor policy as a conditional process of flowing random waypoints to desired robot trajectories. Finally, we introduce a real-world dataset with 10 tasks across Activities of Daily Living to test our framework. Our extensive evaluation highlights that the proposed prompt tuning method for learning manipulation affordance with language prompter achieves competitive performance and even outperforms other finetuning protocols across data scales, while satisfying parameter efficiency. Learning multi-task robot trajectories with flow matching policy also leads to consistently better results than alternative behavior cloning methods, including marginally better generalization performance and prominently faster inference than diffusion policy with DDPM. Our framework seamlessly unifies affordance model learning and trajectory generation with flow matching for robot manipulation. <https://hri-eu.github.io/flow-matching-policy/>.

## 1 Introduction

Recent advances in vision-language models (VLMs) present unprecedented opportunities to solve robot manipulation problems. Attempts in the field have focused on three primary aspects: 1) End-to-end learning manipulation from scratch. These approaches [Padalkar et al., 2023] make the least assumptions on tasks and are formulated in language-image-to-action prediction models. 2) Off-the-shelf-vision-language models for robot manipulation. Such line of works have explored using pre-trained VLMs with prompt engineering in various contexts of robot motion learning, including reward design for reinforcement learning [Ma et al., 2023], python coding [Liang et al., 2023], joint actions [Wang et al., 2023], etc. 3) Intermediate substrate to bridge high-level language-image instructions and low-level robot policies. These works usually introduce some form of prior derived from human knowledge as an intermediate stage, including affordances [Huang et al., 2023], pre-trained visual representations [Xiao et al., 2022], primitive skills [Ingelhart et al., 2024], etc. In this paper, we follow the third line of work to unify an affordance model and low-level robot policies, which helps to alleviate the sample inefficiency problem of end-to-end learning from scratch.

Extracting affordance knowledge has long inspired the robot community [Xiao et al., 2022]. Humans heavily rely on visual affordances to efficiently perform day-to-day tasks across environments. The concept of affordance has been introduced in [Gibson, 2014], referring to the ability to perform certain actions with objects in the context of a given scene. In this work, affordance focuses on the areas of an object that permit or enable specific actions. Affordance models allow more knowledge transfer across different objects with similar affordances, and more intuitive interaction with environments, compared to other intermediate substrates, including keypoints or rewards. We particularly focus on affordance learning in multi-task scenarios with text prompting. As shown in Fig. 1, given the same visual scene

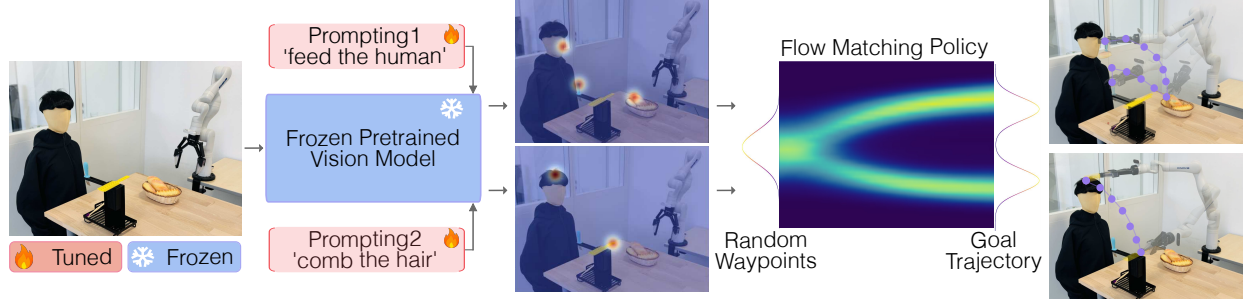


Figure 1: The proposed framework of unifying affordance model learning and trajectory generation for robot manipulation. Given the same visual scene but different language instructions, the model first extracts instruction-relevant manipulation affordances. This is achieved through a prompt tuning method that prepends learnable text-conditioned prompts in a frozen vision foundation model. Then a flow matching policy is proposed to transform the random waypoints to the desired trajectories, guided by task-relevant affordances.

but with different language instructions, we aim to extract different affordances for robot policy learning through our proposed model. To leverage the ability of pre-trained foundation models while avoiding expensive computational constraints, recent works have explored parameter-efficiently fine-tuning (PEFT) large vision-language models for various visual recognition applications [Jia et al., 2022]. PEFT could be mainly categorized into two main groups: adapter-based methods (e. g., LoRA [Hu et al., 2021]) and prompt-based methods [Liu et al., 2023]. One representative line of such research has concentrated on prompt tuning methods, which prepend learnable prompts to the input of a large frozen pre-trained model and optimize them via gradients during finetuning. Studies on randomly-generalized trainable prompts [Jia et al., 2022] for universal use or condition-admitted prompt variables [Sohn et al., 2023] for better specific task performance have been both explored. It has shown that prompt tuning could match the performance of full finetuning but with substantially less parameter storage in various domains, including visual tracking [Zhu et al., 2023] and cross-domain tasks such as language-dance assessment [Zhong and Demiris, 2024]. Inspired in part by the notion of human cognitive penetrability mechanism [Maier and Abdel Rahman, 2019] that uses linguistic knowledge to tune ongoing visual processing, we target to incorporate learnable text-conditioned prompts into any vision foundation model while keeping it frozen, preserving its visual understanding capabilities, to learn instruction-relevant manipulation affordance.

The subsequent challenge involves deploying the visual affordance across various robot manipulation learning paradigms. From the traditional behavior cloning with convolutional networks [Zhang and Demiris, 2022] to transformer-based learning structures [Shridhar et al., 2023], extensive research has modeled robot action trajectories from visual scenes. A recent line of works builds on successes in diffusion models [Chi et al., 2023] to generate motion trajectories to capture multimodal action distributions. Flow Matching is another novel generative method. Sharing theoretical similarities with stochastic Denoising Diffusion Probabilistic Models (DDPM), flow matching aims to regress onto a deterministic vector field to flow samples toward the target distribution. It has proven that the simplicity of flow matching objectives allows favorable performance in stable training and generation quality compared to solving complex stochastic differential equations in DDPM. We extend flow matching to the robotics domain. As shown in Fig. 1 and Fig. 1, the proposed method would flow the random waypoints to the desired trajectories based on various affordances in a single flow matching policy.

We also construct a real-world dataset with 10 tasks across Activities of Daily Living to test the proposed method. The novelty of our dataset is that it contains the same scenarios but with multi-task affordance and robot trajectories. Experimental evaluation on our dataset and other benchmarks empirically demonstrates that the prompt tuning method for learning affordances achieves performance competitive, and sometimes beyond other finetuning protocols across data scales, vision-language fusion architectures, and prompt variants. Furthermore, we showcase that flow matching policy attains favorable performance in stable training, generation quality and computational efficiency amongst competing methods of robot behavior cloning.

This is the first attempt to ground VLM-based affordance with flow matching for real-world robot manipulation. Note that our goal is not to achieve the state-of-the-art general robot manipulation performance, but instead to broadly explore a new paradigm of efficiently adapting VLMs for affordance learning, and robot policy for multimodal action distributions.

The main contributions can be summarized as follows:

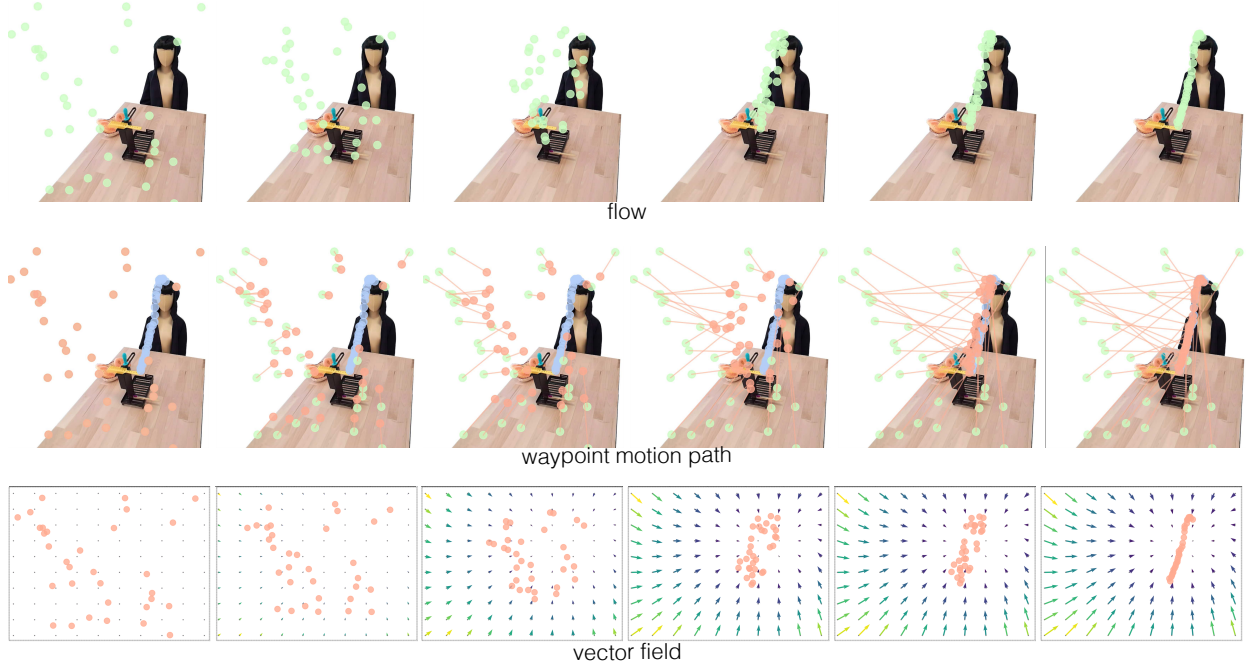


Figure 2: Flow Matching policy representations. The flow, waypoint motion path, and vector field are presented to showcase the process of flow matching transforming random waypoints to the target trajectory from timestep 0 to 1.

1. A parameter-efficient prompt tuning method for adapting pretrained vision foundation model conditioned on language instructions to learn manipulation affordances.
2. A novel formulation using Flow Matching for robot manipulation policy learning from visual affordances.
3. Empirical results show that flow matching policy leads to consistently better results than alternative behavior cloning methods, including marginally better generalization performance and prominently faster inference than diffusion policy with DDPM.

## 2 Related Work

### 2.1 Robot Learning from Demonstration

Imitation learning has been a common paradigm for robots which requires simulated or real-world demonstration data collection [Zhang and Demiris, 2023]. To improve data efficiency, extensive works have been proposed to learn robot policies on the top of visual representations [Liu et al., 2024] instead of end-to-end raw images [Goyal et al., 2023]. Keypoints or affordance heatmaps are often used to provide contact information as visual representation [Liu et al., 2024]. This paper concentrates on using affordances to guide the low-level robot manipulation. In terms of network architectures for robot learning, prior works have successfully investigated convolutional networks [Zhang and Demiris, 2022], Transformers [Shridhar et al., 2023], generative adversarial networks [Ho and Ermon, 2016], Energy-Based Models [Florence et al., 2022], etc. However, the collected data is usually expected to be non-convex and multi-modal due to the variability in human demonstrations. Recent works have addressed this problem by reformulating the robot policy as a generative process. Diffusion policy [Chi et al., 2023] has emerged as a powerful class of generative models for behavior cloning by representing a robot’s visuomotor policy as a conditional denoising diffusion process. In this work, we investigate Flow Matching [Lipman et al., 2022], a novel generative model that has demonstrated its superiority in image generation, but is much less explored in robotics domains.

### 2.2 Parameter-Efficient Finetuning

Instruction-aware vision encoding [Gupta et al., 2022] has been extensively studied for various language-vision fusing tasks [Radford et al., 2021]. Given the dominance of large-scale vision-language models, many approaches have been proposed to efficiently finetune a frozen pretrained model for different downstream tasks to speed up training and

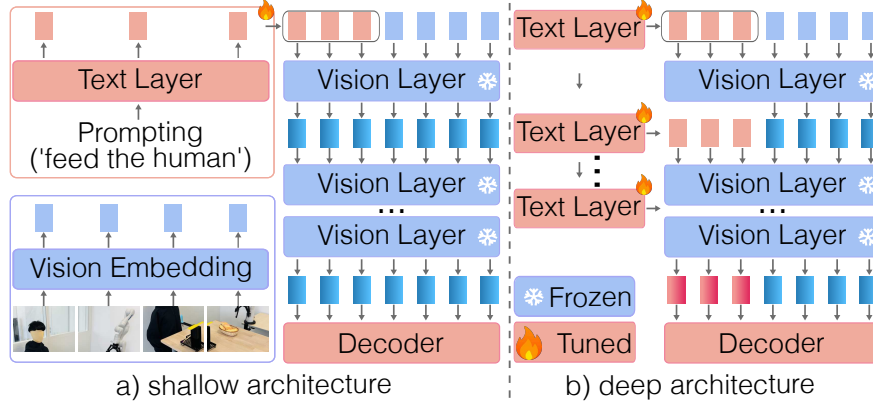


Figure 3: Overview of prompt tuning structures used for affordance learning. (Left) For the shallow structure, text-conditioned prompts are prepended to the first vision transformer layer. (Right) For the deep structure, prompts are inserted to every vision layer. Only the prompt-related layers and the decoder are being updated during the training, while the vision transformer remains frozen.

reduce memory. Two representative methods among them are adapters and prompting. The first type of research varies depending on the adapter that could add extra lightweight modules [Gao et al., 2024] or express the weight updates as a low-rank decomposition of the weight matrix [Hu et al., 2021]. Another line of work focuses on prompting [Liu et al., 2023], which originally primes a frozen pretrained language model for downstream tasks by including a text prompt. Recent works on prompt tuning [Liu et al., 2021] treat prompts as continuous vectors and compute their gradients with backpropagation during training. The extension of prompt tuning to vision tasks has gained massive success. Visual prompt tuning [Jia et al., 2022] has manipulated visual prompts to steer models in arbitrary vision tasks. Other works [Sohn et al., 2023] have further explored extending the random learnable prompts to condition-based prompts (e. g., class, instance) that are hence less universal but more accurate. Inspired by its recent success, we extend the prompt tuning technologies to address the challenge of adapting large pretrained vision-language models to affordance learning for robot manipulation. The intuition is clear: if the model understands the posed text instruction and the inherent context, it should extract visual affordances that directly correspond to the relevant image aspects. Our method achieves the above goal by integrating learnable text-conditioned prompts into a large vision encoder, while keeping it frozen to preserve visual understanding capabilities.

### 2.3 Flow Matching in Robotics

Despite its recent progress in image generation [Albergo and Vanden-Eijnden, 2022], the application of flow matching in robotics domains remains underexplored. Few prior studies [Braun et al., 2024, Hu et al., 2024, Rouxel et al., 2024] have successfully modeled transformations that smoothly move random samples towards target robot actions. These works are nevertheless limited to simulation tasks or conditioned on state-based input. We propose the flow matching policy to learn multi-task robot behavior from raw images with visual affordances in a single supervised policy.

## 3 Methods

### 3.1 Prompt Tuning for Affordance Learning

Given a pre-trained vision transformer, our objective is to learn a set of text-conditioned prompts to maximize the likelihood of correct affordance labels, as shown in Fig. 3. Only the prompt-related layers and the decoder are being updated during the training, while the vision transformer remains frozen. Inspired by Vision Prompt Tuning [Jia et al., 2022], we also propose shallow and deep network architectures.

#### 3.1.1 Shallow Architecture

The vision transformer layer takes the image patch embeddings  $E_0$  as input and passes through various layers  $L_i^v$  to achieve vision features  $E_i$ , where  $E_i \in \mathbb{R}^{M \times C}$  and  $C$  is the channel dimension.

$$E_i = L_i^v(E_{i-1}) \quad i = 1, 2, \dots, N$$

Similarly, the text transformer layer could be represented as

$$\mathbf{P}_i = \mathbf{L}_i^p(\mathbf{P}_{i-1}) \quad i = 1, 2, \dots, N$$

where  $\mathbf{P}_0$  denotes the text tokens, text features  $\mathbf{P}_i$  are obtained through various layers  $\mathbf{L}_i^p$ , where  $\mathbf{p}_i \in \mathbb{R}^{K \times C}$ .

As shown in Fig. 3, for the shallow structure, only one text transformer layer is used to compute text features  $\mathbf{P}_1$ , which are then treated as prompts and inserted into the first vision transformer Layer:

$$\begin{aligned} [\mathbf{Z}_1, \mathbf{E}_1] &= \mathbf{L}_1^v([\mathbf{P}_1, \mathbf{E}_0]) \\ [\mathbf{Z}_i, \mathbf{E}_i] &= \mathbf{L}_i^v([\mathbf{Z}_{i-1}, \mathbf{E}_{i-1}]) \end{aligned}$$

Then a decoder is added on the global output flattened token sequence to generate visual affordance tokens.

$$\text{Affordance} = \text{Decoder}(\mathbf{Z}_N, \mathbf{E}_N)$$

### 3.1.2 Deep Architecture

For the deep architecture, the only difference is that text features  $\mathbf{P}_i$  are computed through each layer and introduced at the corresponding vision transformer layer’s input space:

$$\begin{aligned} [\_, \mathbf{E}_1] &= \mathbf{L}_1^v([\mathbf{P}_1, \mathbf{E}_0]) \\ [\_, \mathbf{E}_i] &= \mathbf{L}_i^v([\mathbf{P}_i, \mathbf{E}_{i-1}]) \end{aligned}$$

### 3.1.3 Implementation Details

Our goal is to integrate textual representations into any vision encoder while keeping it frozen, preserving its visual understanding capabilities. Thus, we have chosen the most basic vision backbone, a pretrained ViT-B-16 transformer. The text layer adopts the classic CLIP setup, including Multiheaded Self-Attention, Feed-Forward Networks with LayerNorm and residual connections. As suggested by MAE [He et al., 2022], the decoder is only used for downstream tasks and could be flexible and lightweight. Thus we use one single transformer decoder layer.

We adopt the L2 Mean Squared loss between the predicted and ground truth affordances for network training. We add positional embeddings to all the image and language tokens to preserve the positional information. In the subsequent experiments, we will further study multiple model variants, including text and vision fusion, prompt depth, pretrained weights for vision transformer, etc.

## 3.2 Flow Matching Policy

We build the robot behavioral cloning policy as a generative process of Flow Matching, which constructs a flow vector that continuously transforms a source probability distribution toward a destination distribution. Flow Matching leverages an ordinary differential equation to deterministically mold data distribution, contrasting with diffusion policy which is based on a stochastic differential equation through introducing noise.

### 3.2.1 Flow Matching Model

Given a conditional probability density path  $p_t(\mathbf{x}|\mathbf{z})$  and a corresponding conditional vector field  $\mathbf{u}_t(\mathbf{x}|\mathbf{z})$ , the objective loss of flow matching could be described as:

$$\mathcal{L}_{\text{FM}}(\boldsymbol{\theta}) = \mathbb{E}_{t, q(\mathbf{z}), p_t(\mathbf{x}|\mathbf{z})} \|\mathbf{v}_t(\mathbf{x}, \boldsymbol{\theta}) - \mathbf{u}_t(\mathbf{x}|\mathbf{z})\|^2 \quad (1)$$

where  $\mathbf{x} \sim p_t(\mathbf{x}|\mathbf{z})$ ,  $t \sim \mathcal{U}[0, 1]$  (uniform distribution). Flow matching aims to regress  $\mathbf{u}_t(\mathbf{x}|\mathbf{z})$  with a time-dependent vector field of flow  $\mathbf{v}_t(\mathbf{x}, \boldsymbol{\theta})$  parameterized as a neural network with weights  $\boldsymbol{\theta}$ .  $\mathbf{u}_t(\mathbf{x}|\mathbf{z})$  can be further simplified as:

$$\mathbf{u}_t(\mathbf{x}|\mathbf{z}) = \mathbf{x}_1 - \mathbf{x}_0 \quad \mathbf{x}_0 \sim p_0, \mathbf{x}_1 \sim p_1$$

$p_0$  represents a simple base density at time  $t = 0$ ,  $p_1$  denotes the target complicated distribution at time  $t = 1$ ,  $\mathbf{x}_0$  and  $\mathbf{x}_1$  are the corresponding samplings.  $\mathbf{v}_t(\mathbf{x}, \boldsymbol{\theta})$  could be described as

$$\mathbf{v}_t(\mathbf{x}, \boldsymbol{\theta}) = v_{\boldsymbol{\theta}}(\mathbf{x}_t, t) \quad (2)$$

We define  $\mathbf{x}_t$  as the linear interpolation between  $\mathbf{x}_0$  and  $\mathbf{x}_1$  with respect to time  $\mathbf{x}_t = t\mathbf{x}_1 + (1-t)\mathbf{x}_0$ , following the Optimal Transport theory [Peyré et al., 2019]. And  $v_{\boldsymbol{\theta}}$  is a network of the flow model. Thus Equation (1) could be reformatted as

$$\mathcal{L}_{\text{FM}}(\boldsymbol{\theta}) = \mathbb{E}_{t, \sim p_0, \sim p_1} \|v_{\boldsymbol{\theta}}(\mathbf{x}_t, t) - (\mathbf{x}_1 - \mathbf{x}_0)\|^2 \quad (3)$$

This represents the progression of the scalar flow that transforms data from source to target between time 0 and 1.



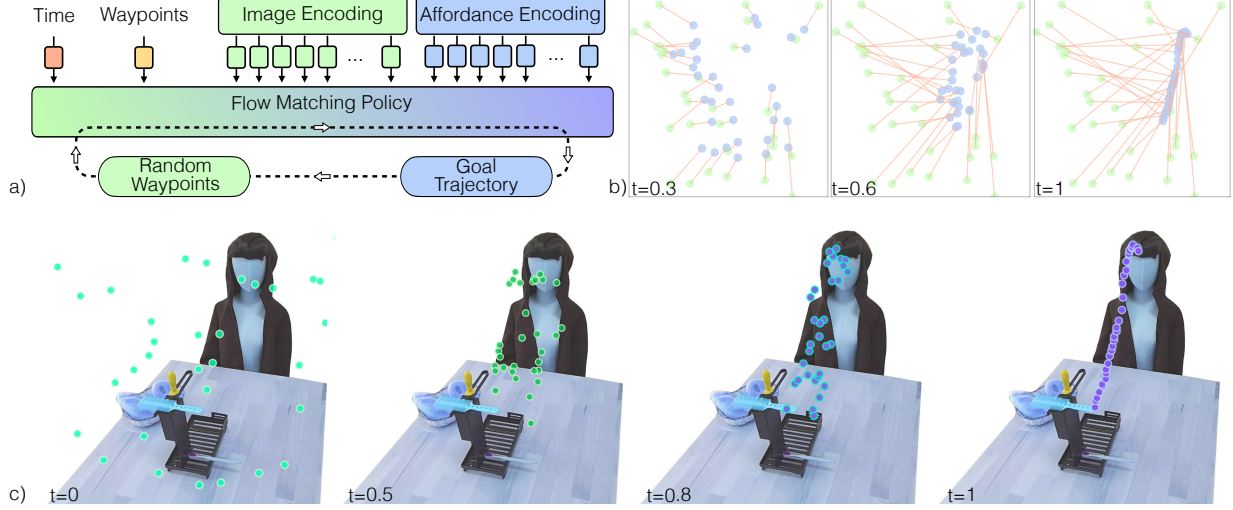


Figure 4: Framework of Flow Matching Policy. (a) At each time step, the policy predicts flow vectors for each waypoint conditioned on visual observation data as well as the waypoints at the current timestep. (b-c) Visualization of the inference phase using Flow matching to transform random waypoints (green) to the target action trajectory (purple) from timestep 0 to 1. The lines in (b) denote the flow vectors.

### 3.2.2 Flow Matching for Visuomotor Policy Learning

We extend flow matching to learn robot visuomotor policies. This requires two modifications in the formulation: i) modeling the flow estimation conditioned on input observations  $\mathbf{o}$ ; ii) changing the output  $\mathbf{x}$  to represent robot actions. Fig. 4 illustrates our model structures.

**Visual observation Conditioning:** We modify Equation (2) to allow the model to predict actions conditioned on observations:

$$\mathbf{v}_t(\mathbf{x}|\mathbf{o}) = v_{\theta}(\mathbf{x}_t, t|\mathbf{o})$$

The visual embeddings  $\mathbf{o}$  are obtained through ResNet [He et al., 2016]. We also evaluate the Transformer structure in our experiments. Various types of inputs include state-based inputs, RGB images, and visual affordances.

**Closed-loop action trajectory prediction:** We execute the action trajectory prediction obtained by our flow matching model for a fixed duration before replanning. At each step, the policy takes the observation data  $\mathbf{o}$  as input and predicts  $T_p$  steps of actions, of which  $T_a$  steps of actions are executed on the robot without re-planning.  $T_p$  is the action prediction horizon and  $T_a$  is the action execution horizon. The policy predicts flow vectors  $\mathbf{v}_t$  conditioned on visual observation data  $\mathbf{o}$  with Feature-wise Linear Modulation (FiLM) [Perez et al., 2018] as well as the interpolated waypoints  $\mathbf{x}_t$ . The flow model  $f_{\theta}$  is represented with U-Net [Ronneberger et al., 2015]. The whole training process of the flow matching policy is illustrated in Algorithm 1. In the subsequent experiments, we will further study multiple model variants, including transformer-based structure, trajectory horizon, etc.

In our case of robot manipulation,  $\mathbf{x}_1$  in Equation (3) represents the demonstration robot action trajectories.  $\mathbf{x}_0$  is the random generated waypoints following a multivariate normal distribution  $\mathbf{x}_0 \sim \mathcal{N}(0, I)$ .  $\mathbf{x}$  here could denote 6D robot end-effector trajectories or robot joint actions.

**Inference:** For the inference procedure, random waypoints are sampled from the source distribution and then flowed into the target trajectory by estimating the flow from  $t = 0$  to  $t = 1$  over steps:

$$\mathbf{x}_{t+\Delta t} = \mathbf{x}_t + \Delta t f(\mathbf{x}_t, t|\mathbf{o}), \quad \text{for } t \in [0, 1] \quad (4)$$

### 3.2.3 Intriguing Properties of Flow Matching Policy

In this section, we provide some insights and intuitions about flow matching policy and its comparisons against diffusion policy for clarification. Algorithm 1 and Algorithm 2 respectively shows the pseudocode of training flow matching and diffusion policy with Denoising Diffusion Probabilistic Models (DDPM). We could see several differences between these two methods:

1. By solving a Stochastic Differential Equation (SDE), DDPM generates a clean sample from Gaussian noise. Flow matching regresses onto a target flow vector field that generates a deterministic mapping from source to target data distributions by solving an ordinary differential equation (ODE).
2. DDPM reverses a diffusion process that adds noise to a clean sample until it becomes Gaussian noise. Flow matching drops all the Gaussian assumptions.
3. Flow matching also includes a particularly interesting family of probability paths: the vector field that corresponds to the principle of Optimal Transport (OT) with linear interpolant. Paths with linear interpolation are simpler than diffusion paths, forming straight line trajectories whereas diffusion paths result in curved paths. These properties seem to empirically translate to more stable training, faster generation, and better performance.

**Algorithm 1** Robot Flow Matching Policy Training

**Input:** observation  $\mathbf{o}$ , target robot actions  $\mathbf{x}_1$ , source random waypoints  $p_0$   
**Output:** flow  $\mathbf{v}_\theta$   
**while** not converged **do**  
 $\mathbf{x}_0 \sim p_0$ , sample random robot waypoints  
 $t \sim \mathcal{U}[0, 1]$ , sample time steps  
 $\mathbf{x}_t = t\mathbf{x}_1 + (1 - t)\mathbf{x}_0$ , linear interpolation  
 $\mathbf{v}_t(\mathbf{x}|\mathbf{o}) = v_\theta(\mathbf{x}_t, t|\mathbf{o})$ , flow estimation  
 $\nabla_\theta \|v_\theta(\mathbf{x}_t, t|\mathbf{o}) - \dot{\mathbf{x}}_t\|$ , gradient step  
**end while**  
 Stopping criteria: 1,000 training epochs

**Algorithm 2** Robot Diffusion Policy (DDPM) Training

**Input:** observation  $\mathbf{o}$ , target robot actions  $\mathbf{x}_1$ , source Gaussian noises  $p_0$   
**Output:** noise  $\epsilon_\theta$   
**while** not converged **do**  
 $\mathbf{x}_0 \sim p_0$ , sample Gaussian noises  
 $t \sim \mathcal{U}[0, 1]$ , sample time steps  
 $\mathbf{x}_t = \mathcal{N}(\mathbf{x}_t; \sqrt{\bar{\alpha}_t}\mathbf{x}_0, (1 - \bar{\alpha}_t)\mathbf{I})$ , forward process  
 $\epsilon_t(\mathbf{x}|\mathbf{o}) = \epsilon_\theta(\mathbf{x}_t, t|\mathbf{o})$ , noise estimation  
 $\nabla_\theta \|\epsilon_\theta(\mathbf{x}_t, t|\mathbf{o}) - \epsilon_t\|$ , gradient step  
**end while**  
 Stopping criteria: 1,000 training epochs

### 3.3 Activities of Daily Living Dataset

We construct a real-world dataset with 10 tasks across Activities of Daily Living to test the proposed method. Each task includes 1,000 sets of RGB images, demonstrated robot trajectories, and labeled ground truth of affordances. Thus 10,000 demonstrations have been collected in total. The data has been manually collected by moving robot end-effectors with kinesthetic teaching. We label the heatmap affordance of our data with 2D Gaussian blobs centered on the pixel of demonstrated action during data collection. The novelty of our dataset could be summarized as: (i) It contains the same scenarios with multiple objects, multi-task affordances, and the demonstrated robot trajectories. (ii) All tasks are related to Activities of Daily Living that involve (simulated) human data.

Objects are randomly placed within the range of the table (1.5 meters  $\times$  1 meter). The human (manikin) is placed randomly around the table in the camera view. We have around 30 different objects. The camera view is fixed as we have not used 3D representation, which will be addressed in our future work.

Our tasks include prompt primitives: ‘sweep the trash’, ‘pass the water to the human’, ‘hang the towel’, ‘put on the hat’, ‘cover the food’, ‘wipe the nose’, ‘wipe the forearm’, ‘feed the human’, ‘comb the hair’, and ‘brush the teeth’. Each task corresponds to one prompt primitive. We could also add a pretrained LLM layer (e. g., GPT) in the front for zero-shot text classification, allowing for linking other language instructions to one of the ten prompt primitives. The dataset will be made publicly available soon.

## 4 Experiments

We systematically evaluate prompt tuning method and flow matching policy against baseline studies. We also investigate how design choices would affect their performance. We randomly split the Activities of Daily Living dataset with 80%-20% percentage of training and testing. The results reported here are obtained after 1,000 epochs of training with 3-fold cross validation to minimize the impact of any noises.

### 4.1 Affordance Evaluation with Prompt Tuning

#### 4.1.1 Baseline Studies

In this experiment, we benchmark our proposed shallow and deep prompt tuning structures against several commonly used finetuning and instruction-aware vision encoding protocols.

- Full finetuning: fully update the text and vision transformer layers and the decoder.

Methods		Learnable Params (M) ↓	Affordance Heatmaps ( $\times 10^{-3}$ ) ↓	Heatmap Centers (pixel) ↓
Baselines	Full	153.8	<b>0.76</b>	<b>1.15</b>
	Decoder	3.9	1.51	13.48
	Adapter	19.2	1.17	6.22
	Cross-attention	43.5	1.26	8.89
	side-network	42.7	1.35	9.20
Ours	PT-shallow	8.0	1.42	12.04
	PT-deep (self-supervised weights)	42.1	<b>0.80</b>	<b>2.93</b>
Ablations	PT-deep (supervised weights)	42.1	1.48	10.13
	PT-deep (image output)	42.1	1.56	13.27

Table 1: Results of prompt tuning baseline and ablation studies. We report the number of learnable parameters, the heatmap estimation error (the fourth column) and the heatmap center error (the fifth column). Our method outshines other baselines except for the full finetuning.

- Adapter-based methods: insert MLP layers with residual connections between pretrained frozen transformer layers of vision and language, as customary in the literature [Gao et al., 2024].
- Decoder-based methods: These methods treat the pretrained backbone as a feature extractor with fixed weights during tuning, and only the decoder is tuned, as customary in the literature [He et al., 2016].
- side-network methods: train a text transformer network on the side and append pretrained vision features and sidetuned text features before being fed into the decoder, as customary in the literature [Ganz et al., 2024].
- Cross-attention methods: Similarly to the above side-network methods, the difference here is using cross-attention fusing instead of simple prepending. An example of cross-attention fusing vision and language could be found in the literature [Jiang et al., 2022].

For a fair comparison, all the baselines here use self-supervised pretrained MAE weights on ImageNet-21k dataset for the vision transformer model. In ablation studies, we will investigate different pretrained weights. The training parameters for the prompt tuning network include an image size of  $224 \times 224$ , AdamW with a learning rate of  $1.5e-4$  including Warmup with step-decay, and batch size of 256. The text encoding layers output 76 tokens, as the CLIP method [Radford et al., 2021].

#### 4.1.2 Main Results

Table 1 presents the results of prompt tuning on our testing dataset for affordance learning, comparing against baselines. We use two metrics to evaluate our results: (i) L2 error of affordance heatmap estimation (the fourth column), and (ii) L2 distance between the predicted and ground truth of heatmap centers (the fifth column). For the inference, we fit Gaussian Mixture Models to determine the heatmap centers. The heatmap error is averaged on each map, and the center error is averaged on per center point.

Four observations could be made from this result:

1. The deep structure outperforms the other baselines except for the full finetuning.
2. Full finetuning slightly outperforms deep prompt tuning in terms of heatmap estimation error and heatmap center error. However, the distinction of heatmap center errors (1.78 pixels) remains subtle, given the full image size of  $224 \times 224$ . This outcome is favorable as it indicates that most heatmap errors are caused by the tails of the Gaussian distribution, instead of the center area where the robot actions actually applied on.
3. As expected, the shallow structure performs suboptimally to the deep structure. In the following ablation studies, we will investigate how the prompt depth affects the performance.
4. Generalizability: We also observe that the trained model could be generalized to new objects. For example, the training dataset only includes a manikin. We found out that it generates well on our testing data with real humans. Note that the proposed tuning method is parameter-efficient, it is envisaged that the method could be readily transferred to different tasks with a small amount of task-specific data.

**What do prompts learn?** We show a t-SNE [Van der Maaten and Hinton, 2008] visualization of the embeddings after the last vision transformer layer and before the decoder in Fig. 5. We can see that the points of the same color (e. g.,



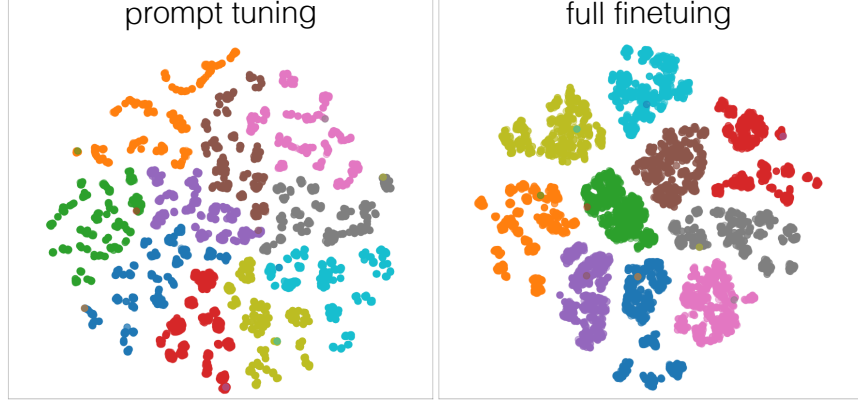


Figure 5: t-SNE visualizations of the embeddings before the decoder. The points of the same color denote the tasks with same language prompts, which are embedded together. The prompt tuning method could produce instruction-relevant features without updating vision backbone parameters.

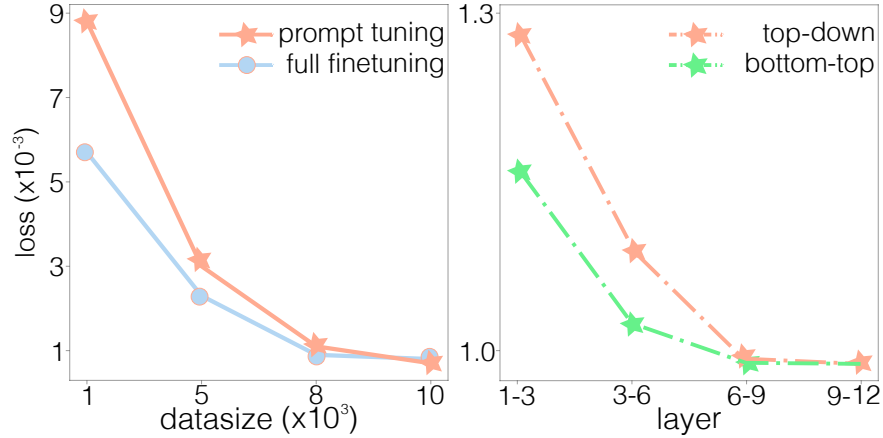


Figure 6: Ablation studies of prompt tuning. We investigate the effect of various design choices on affordance learning performance, including pretrained weights, decoder input, dataset size and prompt location.

tasks with the same language prompts) are embedded together, implying that the representations recover the underlying manifold structure of discriminative task information.

#### 4.1.3 Ablations

We further ablate model design choices.

*Pretrained Weights.* We evaluate using MAE self-supervised pretrained weights and supervised pretrained weights trained on ImageNet-21k dataset for the vision transformer model. The results in Table 1 show self-supervised pretrained weights perform better.

We are aware of other variants of vision transformers or weights, for example, CLIP vision encoder. As our goal is to integrate textual representations into any vision encoder while keeping it frozen, preserving its visual understanding capabilities, we have chosen the most basic ViT-B-16 transformer backbone and commonly used pretrained weights. We have also tried GPT directly, but no constant performance was achieved without carefully designed prompts or finetuning.

*Decoder Input.* We apply the decoder on the global output and image-corresponding output after the vision transformer respectively and report results in Table 1.

*Dataset Size.* We use various amounts of data to train the model. Fig. 6-left shows that prompt tuning has better adaptability than full finetuning when downstream data is scarce.

Methods		2D Trajectory Prediction (pixel) ↓	3D Trajectory Prediction (cm) ↓	Inference Times (ms) ↓
Baselines	Diffusion Policy (2-step inference)	38.37	25.08	24.81
	Diffusion Policy (16-step inference)	0.884	2.096	159.72
	Transformer-based BC	2.797	6.109	7.59
Ours	Flow Matching (Transformer)	2.151	4.842	18.05
	Flow Matching (CNN, 1-step inference)	0.898	2.151	8.53
Ablations	Flow Matching (CNN, 2-step inference)	0.888	2.104	24.29
	Flow Matching (CNN, 4-step inference)	0.846	2.094	44.99
	Flow Matching (CNN, 8-step inference)	0.842	2.092	70.10
	Flow Matching (CNN, 16-step inference)	<b>0.841</b>	<b>2.091</b>	100.98
	Flow Matching (task-specific policy)	1.107	3.41	9.19

Table 2: Results of flow matching policy baseline and ablation studies. We report the error of 2D and 3D trajectory estimation and the average inference time. Our method achieves the best trajectory estimation accuracy, compared to other baselines. We also investigate the effect of various design choices on flow matching performance, including network structure and inference steps.

*Prompt Location.* We have seen different conclusions from prior works about whether the vision-language fusion should be integrated at early or late transformer layers. Thus we conduct experiments to insert prompts at various layers. From Fig. 6-right, we can see that inserting prompts to early layers (for example, layer 1-3 from bottom to top) achieves higher loss than inserting to late layers (for example, layer 1-3 from top to bottom). Thus in our case, prompts have greater significance at the late transformer layers. These results are also supported by the nature of vision transformer hierarchy: lower layers mainly capture low-level fundamental visual details, while higher layers focus on high-level concepts that might be vital for downstream tasks.

In conclusion, we observe no single method that outperforms all the rest. For scenarios where a small number of parameters or datasize is available, we reckon that prompt tuning remains the preferred approach.

## 4.2 Flow Matching Policy Evaluation

### 4.2.1 Baseline Studies

We compare our flow matching policy against two other robot behavior cloning methods: (i) *Diffusion Policy* [Chi et al., 2023] with Denoising Diffusion Probabilistic Models (DDPM), and (ii) *Transformer-based* behavior cloning with Mean Square Error Loss, as customary in RVT [Goyal et al., 2023], RT-X [Padalkar et al., 2023].

Note that we are aware of other well-performed robot behavior cloning methods, including energy-based IBC [Florence et al., 2022], GAIL [Ho and Ermon, 2016], etc. Since extensive studies have been conducted and showed lower performance of these methods compared to diffusion policy, we choose two representative baselines for evaluation.

We consider CNN-based and Transformer-based structures for flow matching. The flow matching and baselines are trained in a supervised manner using RGB images with visual affordances as input, and the output is a long-horizon trajectory in both 2D pixel space and 3D Cartesian space. All 10 tasks in our dataset are trained in a single policy. Table 4 shows the hyperparameters we have used in flow matching and diffusion policy. Table 5 shows the tasks Summary.

### 4.2.2 Main Results

Table 2 presents the results of flow matching policy on our testing dataset for robot trajectory learning, comparing against baselines. We use two metrics for evaluation: (i) the error of 2D and 3D trajectory estimation, and (ii) the average inference time across various steps, performed using PyTorch with RTX 4090 GPU acceleration. The trajectory error is averaged on each point of the trajectory.

Three observations could be made from this result:

1. **Generation Quality:** Flow matching (CNN-based, 16 steps) outperforms other baselines in terms of 2D and 3D trajectory prediction accuracy. The Transformer behavior cloning achieves marginal precision. This is expected as it is hindered by the nature of multi-modal action distribution, causing the averaging out across non-convex spaces.

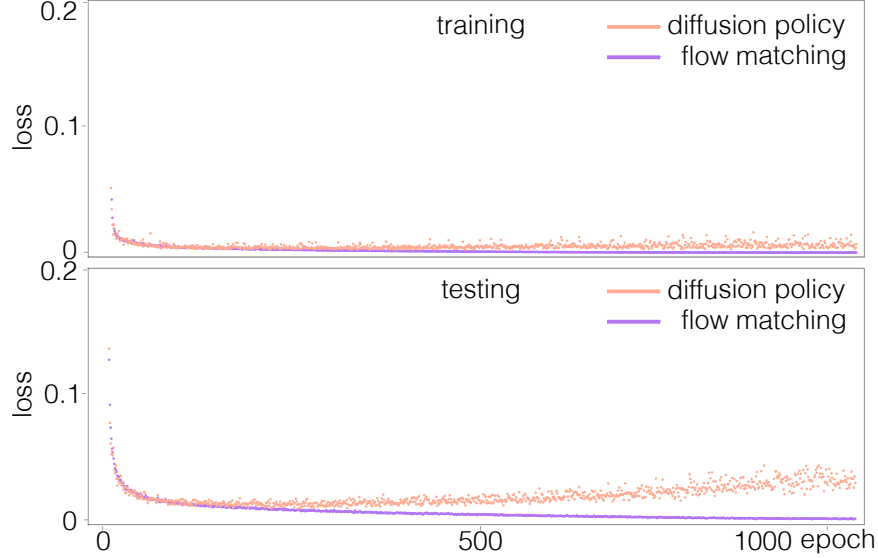


Figure 7: Training and testing loss of flow matching and diffusion policy throughout the training process. Flow matching exhibits greater stability on both training and evaluation than diffusion policy.

2. **Stability:** Fig. 7 shows an example of training and testing loss of flow matching and diffusion policy throughout the training process. We can see flow matching exhibits greater stability on both training and evaluation than diffusion policy.

3. **Inference Time:** In terms of inference time, Table 2 showcases that flow matching with 16 steps achieves faster inference time compared to diffusion policy with 16 steps. We hypothesize that flow matching with linear pointwise flows (following the optimal transport theory) generates straighter flows, and thus causes faster inference. Table 2 also showcases better performances of diffusion policy when applying more inference iterations, with a trade-off of longer inference time. Contrarily, flow matching has not shown significant improvements when increasing inference steps. We hypothesize that this is because flow matching trains Continuous Normalizing Flow models, where an ordinary differential equation is solved without learning a series of discrete steps to progressively refine the generated sample. This considerably reduces the inference time for closed-loop robot manipulation, as 2-step flow matching (error: 0.888cm, time: 8.53ms) has achieved comparable performance as 16-step diffusion policy (error: 0.884cm, time: 159.72ms), but prominently lower inference time roughly by 85%.

#### 4.2.3 Real-World Robot Experiments

We deploy flow matching and other policies on real robot manipulation evaluation, as shown in Table 3. We carry out 50 replications of trials for each policy. The orientation is predefined. We use a KINOVA Gen3 arm, an Azure Kinect camera, and a 3D printed UMI gripper [Chi et al., 2024] for real-world robot experiments.

We observe that most failures occurred during the initial grasping. Even the trajectory prediction is accurate in general, a slight misalignment between the first trajectory waypoint and the object would cause grasping failures. This problem might be addressed in the future by a weighted flow matching policy, which highlights the initial waypoints by adding higher probability weights. Some out-of-distribution factors also lead to failure, including background and camera view changes. Larger data sizes and more diversity should alleviate this problem.

**RGB images ablations against affordances:** We also investigate how the affordance would guide the flow matching policy. We trained flow matching for each task separately, taking the raw RGB images as input. It achieves a higher loss but a similar success rate compared to training all tasks in one policy with affordance guidance. Interestingly, a further comprehensive examination reinforces the argument that flow matching could handle multimodal action distribution. Fig. 8 shows an example. From the left figure, we can see that when training a separate policy of moving the towel toward the trash for sweeping, the predicted trajectory (yellow) could be detached from the ground truth (red), but still a reasonable solution that allows for a successful robot execution. With affordance guidance, the prediction is closely aligned with the truth (Fig. 8-right).



Figure 8: Ablations between using RGB images and affordances as inputs. We show examples of how visual affordance guides the flow matching policy.

#### 4.2.4 Ablations

We further ablate various policy design choices.

*Network Structure:* As shown in Table 2, CNN-based flow matching achieves better results than transformer-based architecture. We hypothesize that transformer might need additional hyperparameter tuning.

*Trajectory Horizon:* We empirically test trajectory representation with 8, 16, 32 and 64 waypoints. More waypoints are not necessary, while fewer waypoints are unable to entirely encapsulate the complete long-horizon trajectories. We have found that, in general, the trajectory horizon does not wield a significant influence on flow matching performance. The performance reported in the above main results section is achieved by using 32 waypoints to represent the trajectory.

### 4.3 Comparisons between flow matching policy diffusion policy

To further investigate the performance of flow matching compared to diffusion policy, we benchmark the proposed methods on two more datasets: (i) **Push-T** adapted from [Florence et al., 2022]; and (ii) **Franka Kitchen** proposed in Relay Policy Learning [Gupta et al., 2019].

1. **Push-T** requires pushing a T-shaped block to a fixed target with a circular end-effector. Push-T takes RGB images with proprioception of end-effector location as inputs, and end-effector actions as outputs. The experiments are carried out in a closed-loop manner. All methods are trained with 200 demonstrations for 3,000 epochs. Variation is added by random initial conditions for T block and end-effector.

2. **Franka Kitchen** contains 7 objects for interaction and comes with a human demonstration dataset of 566 demonstrations, each completing 4 tasks in arbitrary order. The goal is to execute as many demonstrated tasks as possible, regardless of order, showcasing both short-horizon and long-horizon multimodality. The training takes states as inputs, and robot joint actions as outputs for 4,500 epochs. This benchmark includes 6D closed-loop robot position and orientation actions, as well as gripper actions. Variation is added by random initial conditions for the robot and object states.

For Push-T and Franka Kitchen benchmarks, we report results from the average of the last checkpoint with 10 trials of replication. In addition, we also report the best performance in the replications of the last checkpoint. The evaluation is carried out across 500 different environment initial conditions (5,000 in total).

3. **Real-world Daily Living Task**, for clarity, takes affordance images as inputs, and 3D position end-effector trajectories as outputs. One-shot open-loop estimation of the entire trajectory is used in our dataset. We randomly split the dataset with 80%-20% percentage of training and testing. The results reported are obtained after 1,000 epochs of training with 3-fold cross validation to minimize the impact of any noises. Other training and testing details have been illustrated in the above sections.

Table 4 shows the hyperparameters we have used in flow matching and diffusion policy. Table 5 shows the tasks Summary.

Similar conclusions could be achieved from Table 3, as in the Main Results section: (i) **Generation Quality**: Flow matching outperforms diffusion policy in all benchmarks of robot manipulation experiments. (ii) **Inference Time**: Flow matching considerably reduces the inference time for closed-loop robot manipulation. For example, in Franka Kitchen benchmark, 2-step flow matching (success rate: 0.9750, time: 13.18ms) has achieved comparable performance as 16-step diffusion policy (success rate: 0.9840, time: 157.46ms), but prominently lower inference time roughly by 90%.

Methods (Inference Step)	Flow Matching (2-step) $\uparrow$	Diffusion Policy (2-step) $\uparrow$	Flow Matching (16-step) $\uparrow$	Diffusion Policy (16-step) $\uparrow$	Transformer BC $\uparrow$	Flow Matching separate policy
Push-T	0.8771/0.7111	0.4412/0.1872	<b>0.9035/0.7490</b>	0.8840/0.7178	—	—
Franka Kitchen	0.9750/0.6134	0.2355/0.0527	<b>0.9960/0.7172</b>	0.9840/0.6716	—	—
Real-world Daily Living Task	—	—	<b>0.82</b>	0.76	0.44	0.80

Table 3: We present the robot performance with different checkpoint selection methods in the format of (max performance) / (average of last checkpoint with 10 trials of replication), with each averaged across 500 different environment initial conditions (5000 in total) for testing. The metric used here is success rate, except for the Push-T task which uses target area coverage.

DDPM	Ta	Tp	ImgRes	D-Net	D-Para	V-Enc	V-Para	Lr	WDecay	Iters Train	Iters Eval
Push-T	8	16	96x96	ConditionalUnet1D	73	ResNet-18	12	1e-4	1e-6	16	2/4/8/16
Franka Kitchen	8	16	N/A	ConditionalUnet1D	73	N/A	N/A	1e-4	1e-6	16	2/4/8/16
Real-world Daily Living Task	32	32	224x224	ConditionalUnet1D	73	ResNet-18	12	1e-4	1e-6	16	2/4/8/16
Flow Matching	Ta	Tp	ImgRes	F-Net	F-Para	V-Enc	V-Para	Lr	WDecay	Iters Train	Iters Eval
Push-T	8	16	96x96	ConditionalUnet1D	73	ResNet-18	12	1e-4	1e-6	N/A	2/4/8/16
Franka Kitchen	8	16	N/A	ConditionalUnet1D	73	N/A	N/A	1e-4	1e-6	N/A	2/4/8/16
Real-world Daily Living Task	32	32	224x224	ConditionalUnet1D	73	ResNet-18	12	1e-4	1e-6	N/A	2/4/8/16

Table 4: Hyperparameters for flow matching and Diffusion Policy. Ta: action horizon. Tp: action prediction horizon. ImgRes: environment observation resolution. D-Net: diffusion network. D-Para: diffusion network number of parameters in millions. F-Net: flow matching network. F-Para: flow matching network number of parameters in millions. V-Enc: vision encoder. V-Para: vision encoder number of parameters in millions. Lr: learning rate. WDecay: weight decay. Iters Train: number of training diffusion iterations. Iters Eval: number of inference iterations. Network structures for flow matching policy are modified in the same way in diffusion policy.

Tasks	Rob	Obj	ActD	PH	Steps	Img	Closed-loop
Push-T	1	1	2	200	300	✓	✓
Franka Kitchen	1	7	9	566	280	✗	✓
Real-world Daily Living Task	1	≈ 30	3	8,000	N/A	✓	✗

Table 5: Tasks Summary. Rob: number of robots. Obj: number of objects. ActD: action dimension. PH: proficient-human demonstration. Steps: max number of rollout steps.

## 5 Conclusion

We have formulated a prompt tuning method for affordance learning and flow matching policy for robot manipulation. The core idea of prompt tuning is to maximally exploit the pretrained foundation model, and rapidly excavate the relevance of foundation and downstream affordance learning tasks. Our focus in this work is not to outperform state-of-the-art general robot manipulation research. Instead, we have systematically studied flow matching framework, which provides an alternative to diffusion policy. The results suggest forsaking the stochastic construction in favor of learning the probability path more directly, allowing for improved generation and faster inference. We qualitatively and quantitatively experiment on the multi-task robot manipulation scenarios to prove the ease of training and evaluation for flow matching.

The 3D estimation performs decently with our method using only RGB images as input. But we also observe the 3D estimation could be highly attuned to camera angles. We could further improve performance by incorporating depth or pointcloud information for 3D orientation modeling. We leave these for future work.

## References

- Abhishek Padalkar, Acorn Pooley, Ajinkya Jain, Alex Bewley, Alex Herzog, Alex Irpan, Alexander Khazatsky, Anant Rai, Anikait Singh, Anthony Brohan, et al. Open x-embodiment: Robotic learning datasets and rt-x models. *arXiv preprint arXiv:2310.08864*, 2023.
- Yecheng Jason Ma, William Liang, Guanzhi Wang, De-An Huang, Osbert Bastani, Dinesh Jayaraman, Yuke Zhu, Linxi Fan, and Anima Anandkumar. Eureka: Human-level reward design via coding large language models. *arXiv preprint arXiv:2310.12931*, 2023.
- Jacky Liang, Wenlong Huang, Fei Xia, Peng Xu, Karol Hausman, Brian Ichter, Pete Florence, and Andy Zeng. Code as policies: Language model programs for embodied control. In *2023 IEEE International Conference on Robotics and Automation (ICRA)*, pages 9493–9500. IEEE, 2023.
- Yen-Jen Wang, Bike Zhang, Jianyu Chen, and Koushil Sreenath. Prompt a robot to walk with large language models. *arXiv preprint arXiv:2309.09969*, 2023.
- Wenlong Huang, Chen Wang, Ruohan Zhang, Yunzhu Li, Jiajun Wu, and Li Fei-Fei. Voxposer: Composable 3d value maps for robotic manipulation with language models. *arXiv preprint arXiv:2307.05973*, 2023.
- Tete Xiao, Ilija Radosavovic, Trevor Darrell, and Jitendra Malik. Masked visual pre-training for motor control. *arXiv preprint arXiv:2203.06173*, 2022.
- Nils Ingelhart, Jesper Munkeby, Jonne van Haastregt, Anastasia Varava, Michael C Welle, and Danica Kragic. A robotic skill learning system built upon diffusion policies and foundation models. *arXiv preprint arXiv:2403.16730*, 2024.
- James J Gibson. *The ecological approach to visual perception: classic edition*. Psychology press, 2014.
- Menglin Jia, Luming Tang, Bor-Chun Chen, Claire Cardie, Serge Belongie, Bharath Hariharan, and Ser-Nam Lim. Visual prompt tuning. In *European Conference on Computer Vision*, pages 709–727. Springer, 2022.
- Edward J Hu, Yelong Shen, Phillip Wallis, Zeyuan Allen-Zhu, Yuanzhi Li, Shean Wang, Lu Wang, and Weizhu Chen. Lora: Low-rank adaptation of large language models. *arXiv preprint arXiv:2106.09685*, 2021.
- Pengfei Liu, Weizhe Yuan, Jinlan Fu, Zhengbao Jiang, Hiroaki Hayashi, and Graham Neubig. Pre-train, prompt, and predict: A systematic survey of prompting methods in natural language processing. *ACM Computing Surveys*, 55(9): 1–35, 2023.
- Kihyuk Sohn, Huiwen Chang, José Lezama, Luisa Polania, Han Zhang, Yuan Hao, Irfan Essa, and Lu Jiang. Visual prompt tuning for generative transfer learning. In *Proceedings of the IEEE/CVF Conference on Computer Vision and Pattern Recognition*, pages 19840–19851, 2023.
- Yiwen Zhu, Simiao Lai, Xin Chen, Dong Wang, and Huchuan Lu. Visual prompt multi-modal tracking. In *Proceedings of the IEEE/CVF conference on computer vision and pattern recognition*, pages 9516–9526, 2023.
- Yun Zhong and Yiannis Demiris. Dancemvp: Self-supervised learning for multi-task primitive-based dance performance assessment via transformer text prompting. In *Proceedings of the AAAI Conference on Artificial Intelligence*, volume 38, pages 10270–10278, 2024.
- Martin Maier and Rasha Abdel Rahman. No matter how: Top-down effects of verbal and semantic category knowledge on early visual perception. *Cognitive, Affective, & Behavioral Neuroscience*, 19:859–876, 2019.
- Fan Zhang and Yiannis Demiris. Learning garment manipulation policies toward robot-assisted dressing. *Science robotics*, 7(65):eabm6010, 2022.
- Mohit Shridhar, Lucas Manuelli, and Dieter Fox. Perceiver-actor: A multi-task transformer for robotic manipulation. In *Conference on Robot Learning*, pages 785–799. PMLR, 2023.
- Cheng Chi, Siyuan Feng, Yilun Du, Zhenjia Xu, Eric Cousineau, Benjamin Burchfiel, and Shuran Song. Diffusion policy: Visuomotor policy learning via action diffusion. *arXiv preprint arXiv:2303.04137*, 2023.
- Fan Zhang and Yiannis Demiris. Visual-tactile learning of garment unfolding for robot-assisted dressing. *IEEE Robotics and Automation Letters*, 2023.
- Fangchen Liu, Kuan Fang, Pieter Abbeel, and Sergey Levine. Moka: Open-vocabulary robotic manipulation through mark-based visual prompting. *arXiv preprint arXiv:2403.03174*, 2024.
- Ankit Goyal, Jie Xu, Yijie Guo, Valts Blukis, Yu-Wei Chao, and Dieter Fox. Rvt: Robotic view transformer for 3d object manipulation. In *Conference on Robot Learning*, pages 694–710. PMLR, 2023.
- Jonathan Ho and Stefano Ermon. Generative adversarial imitation learning. *Advances in neural information processing systems*, 29, 2016.



- Pete Florence, Corey Lynch, Andy Zeng, Oscar A Ramirez, Ayzaan Wahid, Laura Downs, Adrian Wong, Johnny Lee, Igor Mordatch, and Jonathan Tompson. Implicit behavioral cloning. In *Conference on Robot Learning*, pages 158–168. PMLR, 2022.
- Yaron Lipman, Ricky TQ Chen, Heli Ben-Hamu, Maximilian Nickel, and Matt Le. Flow matching for generative modeling. *arXiv preprint arXiv:2210.02747*, 2022.
- Tanmay Gupta, Amita Kamath, Aniruddha Kembhavi, and Derek Hoiem. Towards general purpose vision systems: An end-to-end task-agnostic vision-language architecture. In *Proceedings of the IEEE/CVF Conference on Computer Vision and Pattern Recognition*, pages 16399–16409, 2022.
- Alec Radford, Jong Wook Kim, Chris Hallacy, Aditya Ramesh, Gabriel Goh, Sandhini Agarwal, Girish Sastry, Amanda Askell, Pamela Mishkin, Jack Clark, et al. Learning transferable visual models from natural language supervision. In *International conference on machine learning*, pages 8748–8763. PMLR, 2021.
- Peng Gao, Shijie Geng, Renrui Zhang, Teli Ma, Rongyao Fang, Yongfeng Zhang, Hongsheng Li, and Yu Qiao. Clip-adapter: Better vision-language models with feature adapters. *International Journal of Computer Vision*, 132(2): 581–595, 2024.
- Xiao Liu, Kaixuan Ji, Yicheng Fu, Weng Lam Tam, Zhengxiao Du, Zhilin Yang, and Jie Tang. P-tuning v2: Prompt tuning can be comparable to fine-tuning universally across scales and tasks. *arXiv preprint arXiv:2110.07602*, 2021.
- Michael S Albergo and Eric Vanden-Eijnden. Building normalizing flows with stochastic interpolants. *arXiv preprint arXiv:2209.15571*, 2022.
- Max Braun, Noémie Jaquier, Leonel Rozo, and Tamim Asfour. Riemannian flow matching policy for robot motion learning. *arXiv preprint arXiv:2403.10672*, 2024.
- Xixi Hu, Bo Liu, Xingchao Liu, and Qiang Liu. Adaflow: Imitation learning with variance-adaptive flow-based policies. *arXiv preprint arXiv:2402.04292*, 2024.
- Quentin Rouxel, Andrea Ferrari, Serena Ivaldi, and Jean-Baptiste Mouret. Flow matching imitation learning for multi-support manipulation. *arXiv preprint arXiv:2407.12381*, 2024.
- Kaiming He, Xinlei Chen, Saining Xie, Yanghao Li, Piotr Dollár, and Ross Girshick. Masked autoencoders are scalable vision learners. In *Proceedings of the IEEE/CVF conference on computer vision and pattern recognition*, pages 16000–16009, 2022.
- Gabriel Peyré, Marco Cuturi, et al. Computational optimal transport: With applications to data science. *Foundations and Trends® in Machine Learning*, 11(5-6):355–607, 2019.
- Kaiming He, Xiangyu Zhang, Shaoqing Ren, and Jian Sun. Deep residual learning for image recognition. In *Proceedings of the IEEE conference on computer vision and pattern recognition*, pages 770–778, 2016.
- Ethan Perez, Florian Strub, Harm De Vries, Vincent Dumoulin, and Aaron Courville. Film: Visual reasoning with a general conditioning layer. In *Proceedings of the AAAI conference on artificial intelligence*, volume 32, 2018.
- Olaf Ronneberger, Philipp Fischer, and Thomas Brox. U-net: Convolutional networks for biomedical image segmentation. In *Medical image computing and computer-assisted intervention–MICCAI 2015: 18th international conference, Munich, Germany, October 5-9, 2015, proceedings, part III* 18, pages 234–241. Springer, 2015.
- Roy Ganz, Yair Kittenplon, Aviad Aberdam, Elad Ben Avraham, Oren Nuriel, Shai Mazor, and Ron Litman. Question aware vision transformer for multimodal reasoning. In *Proceedings of the IEEE/CVF Conference on Computer Vision and Pattern Recognition*, pages 13861–13871, 2024.
- Yunfan Jiang, Agrim Gupta, Zichen Zhang, Guanzhi Wang, Yongqiang Dou, Yanjun Chen, Li Fei-Fei, Anima Anandkumar, Yuke Zhu, and Linxi Fan. Vima: General robot manipulation with multimodal prompts. *arXiv preprint arXiv:2210.03094*, 2(3):6, 2022.
- Laurens Van der Maaten and Geoffrey Hinton. Visualizing data using t-sne. *Journal of machine learning research*, 9 (11), 2008.
- Cheng Chi, Zhenjia Xu, Chuer Pan, Eric Cousineau, Benjamin Burchfiel, Siyuan Feng, Russ Tedrake, and Shuran Song. Universal manipulation interface: In-the-wild robot teaching without in-the-wild robots. In *Proceedings of Robotics: Science and Systems (RSS)*, 2024.
- Abhishek Gupta, Vikash Kumar, Corey Lynch, Sergey Levine, and Karol Hausman. Relay policy learning: Solving long-horizon tasks via imitation and reinforcement learning. *arXiv preprint arXiv:1910.11956*, 2019.